Journal of Sound and Vibration (1997) **206**(3), 353–369

FREE VIBRATION OF A TIMOSHENKO BEAM PARTIALLY LOADED WITH DISTRIBUTED MASS

K. T. Chan and X. Q. Wang

Department of Mechanical Engineering, The Hong Kong Polytechnic University, Hung Hom, Kowloon, Hong Kong

(*Received* 20 *January* 1997, *and in final form* 18 *April* 1997)

Exact frequencies and mode shapes have been calculated for a Timoshenko beam, on different boundary supports and partially loaded with a distributed mass span. They agree with experimental data. For the higher modes, frequencies obtained through the Euler–Bernoulli theory are not as accurate as the Timoshenko ones. Results show the effects of the added mass length, position and density on natural frequencies. The variation is cyclical with range depending on the added mass inertia. For certain loading, the range of variation is small, showing frequency to be insensitive to added mass location.

1. INTRODUCTION

The Euler–Bernoulli equation only applies to slender beams vibrating at long wavelengths. Rayleigh [1] considered the rotary effect on uniform beam vibration. Timoshenko [2, 3] considered both the rotary inertia and shear deformation effects. Such a beam was, then referred to as the Timoshenko beam. The solutions of Timoshenko's equation for flexural vibration of a uniform beam have been extensively studied. Traill-Nash and Collar [4] presented a fairly complete treatment to this problem. In their study, the frequency equations and mode shape forms of a Timoshenko beam were given for various combinations of three usual types of boundary conditions, namely, free, simply-supported and clamped. They showed the appearance of a new spectrum of natural frequencies above a critical frequency value, and related this to the resonant interaction between the beam inertia rotation and shearing deflection. It was also shown that for a simply-supported beam, there existed a pure shear mode at the critical frequency. For various boundary conditions, Huang [5] obtained two sets of solutions of the Timoshenko equation for total deflection and bending slope. The constants in these two sets of solutions could be related to each other. Two distinct natural frequency spectra were also found in the paper.

In Huang [5], a specific example of a given length of beam showed reduction of modal frequencies with increasing radius of gyration. Frequency reduction was found to be more dominant for thicker beams. It was also evident in his results that the higher the mode, the greater the frequency reduction.

The work mentioned above showed that closed-form solutions existed only for uniform beams on certain types of boundary conditions but were generally non-existent for non-uniform beams. Grant [6] studied vibration of a Timoshenko beam carrying a concentrated mass at an arbitrary position. Using the Dirac δ-function to represent the concentrated mass and Laplace transform, he obtained frequency results that showed reduction of frequency with increasing Timoshenko effect.

0022–460X/97/380353 + 17 $25.00/0/sv971124

Solutions have not been obtained so far for vibration of a Timoshenko beam partially loaded with distributed mass. For a partially loaded Euler–Bernoulli beam, exact solutions have been obtained by Chan and Zhang [7] and Chan *et al*. [8]. The present paper will follow the latter to introduce an exact method to tackle the problem of a Timoshenko beam partially loaded with distributed mass at an arbitrary position. Since there are no published results so far for comparison, experimental data have been produced to validate the model. Computational results will also be given to show some interesting features of frequency variations.

2. TIMOSHENKO BEAM PARTIALLY LOADED WITH DISTRIBUTED MASS

2.1. UNIFORM BEAM WITHOUT LOADED MASS

As a basis for analysis, consider a uniform Timoshenko beam. According to Huang [5], the equations of motion for free bending vibration of a Timoshenko beam can be written as,

$$EI\frac{\partial^2\phi(x,t)}{\partial x^2}+kaG\left(\frac{\partial w(x,t)}{\partial x}-\phi(x,t)\right)-\frac{mI}{a}\frac{\partial^2\phi(x,t)}{\partial t^2}=0, \tag{1a}$$

$$m\frac{\partial^2 w(x,t)}{\partial t^2}-kaG\left(\frac{\partial^2 w(x,t)}{\partial x^2}-\frac{\partial\phi(x,t)}{\partial x}\right)=0, \tag{1b}$$

where $w(x, t)$ is the transverse displacement and $\phi(x, t)$ the slope due to bending. The above equations are coupled. E and G are the Young's and shear moduli, respectively. I is the second moment of area of the cross-section, a is the cross-sectional area and m is the mass per unit length of the beam. k is the shear coefficient depending on the shape of the cross section and the vibration frequency of the beam.

Considerable attention has been paid to the determination of k [9–17]. The results by Cowper [11] appear to be most comprehensive and based on elementary theory of elasticity. In fact, the values of k reported in references 9–17 are within a range that should not affect the calculated frequencies very much, below 2% in the present paper.

The general solutions of equations (1a and 1b) as given by Huang [5] are written as,

$$w(x,t)=W(x)\,e^{j\omega t}=(A\sin k_a x+B\cos k_a x+C\sinh k_b x+D\cosh k_b x)\,e^{j\omega t}, \tag{2}$$

$$\phi(x,t)=\Phi(x)\,e^{j\omega t}=(Aq_a\cos k_a x-Bq_a\sin k_a x+Cq_b\cosh k_b x+Dq_b\sinh k_b x)\,e^{j\omega t}, \tag{3}$$

where ω is the free vibrating frequency of the beam. In the equations, k_a and k_b are expressed as,

$$k_a=(\sqrt{([\alpha-\beta]/2)^2+\eta}+(\alpha+\beta)/2)^{1/2},\qquad k_b=(\sqrt{([\alpha-\beta]/2)^2+\eta}-(\alpha+\beta)/2)^{1/2}, \tag{4a, b}$$

where $\alpha=\omega^2 m/Ea$, $\beta=\omega^2 m/kGa$ and $\eta=\omega^2 m/EI$. The coefficients A, B, C, and D are constants and $q_a=k_a-\beta/k_a$ and $q_b=k_b+\beta/k_b$.

It can be seen that k_a is always real and positive, while k_b may be real, zero, or imaginary, depending on the value of ω^2. This leads to the appearance of two spectra in the frequency domain as mentioned above [4]. Since the aim of this paper is to demonstrate some features of frequency variations with the distributed mass, the problem of two spectra of

frequencies will not be discussed in this paper and the concerned frequencies are limited within the first spectrum of frequencies, that is, k_b is real.

2.2. UNIFORM BEAM WITH LOADED MASS

Consider the beam partially loaded with distributed mass as shown in Figure 1. To simplify the mathematical procedure, the origin of the co-ordinates is now located at the left side of the distributed mass, that is, l_d from the left end of the beam. The lengths of the beam and of the distributed mass are L and l_a, respectively. The equation of motion can be expressed as

$$EI\frac{\partial^2\phi(x,t)}{\partial x^2} + kaG\left(\frac{\partial w(x,t)}{\partial x} - \phi(x,t)\right) - \frac{m(x)I}{a}\frac{\partial^2\phi(x,t)}{\partial t^2} = 0, \tag{5a}$$

$$m(x)\frac{\partial^2 w(x,t)}{\partial t^2} - kaG\left(\frac{\partial^2 w(x,t)}{\partial x^2} - \frac{\partial\phi(x,t)}{\partial x}\right) = 0, \tag{5b}$$

where $m(x)$ is defined as,

$$m(x) = \begin{cases} m & -l_d \leqslant x < 0,\ l_a < x \leqslant L - 1_d, \\ m + m_a & 0 \leqslant x \leqslant l_a \end{cases} \tag{6}$$

where m_a is the added mass per unit length.

Then the general solutions can be written in three parts,

$$w_i(x,t) = W_i(x)\,\mathrm{e}^{\mathrm{j}\omega t} = (A_i \sin k_{ai}x + B_i \cos k_{ai}x + C_i \sinh k_{bi}x + D_i \cosh k_{bi}x)\,\mathrm{e}^{\mathrm{j}\omega t}, \tag{7}$$

$$\begin{aligned}\phi_i(x,t) &= \Phi_i(x)\,\mathrm{e}^{\mathrm{j}\omega t} \\ &= (A_i q_{ai} \cos k_{ai}x - B_i q_{ai} \sin k_{ai}x + C_i q_{bi} \cosh k_{bi}x + D_i q_{bi} \sinh k_{bi}x)\,\mathrm{e}^{\mathrm{j}\omega t},\end{aligned} \tag{8}$$

where $i = 1$ for $-l_d \leqslant x < 0$; $i = 2$ for $0 \leqslant x \leqslant l_a$; and $i = 3$ for $l_a < x \leqslant L - l_d$. In these equations,

$$k_{ai} = (\sqrt{([\alpha_i - \beta_i]/2)^2 + \eta_i} + (\alpha_i + \beta_i)/2)^{1/2}, \tag{9}$$

$$k_{bi} = (\sqrt{([\alpha_i - \beta_i]/2)^2 + \eta_i} - (\alpha_i + \beta_i)/2)^{1/2}; \tag{10}$$

$$\alpha_i = \omega^2 m_i/Ea, \qquad \beta_i = \omega^2 m_i/kGa \quad \text{and} \quad \eta_i = \omega^2 m_i/EI; \qquad m_1 = m_3 = m$$

and

$$m_2 = m + m_a;$$

$$q_{ai} = k_{ai} - \beta_i/k_{ai} \text{ and } q_{bi} = k_{bi} + \beta_i/k_{bi}.$$

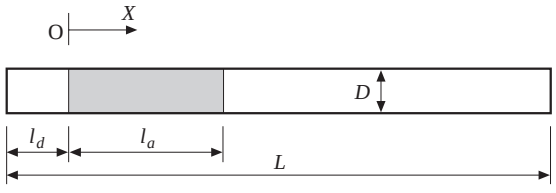

Figure 1. Schematic diagram of the Timoshenko beam partially loaded with distributed mass.

When the three sections are split, the continuity and equilibrium conditions at the two ends of the distributed mass give the following two groups of equations,

$$w_1(0, t) = w_2(0, t). \qquad \phi_1(0, t) = \phi_2(0, t), \qquad EI\phi_1'(0, t) = EI\phi_2'(0, t),$$
$$kaG(w_1'(0, t) - \phi_1(0, t)) = kaG(w_2'(0, t) - \phi_2(0, t)), \tag{11}$$

and

$$w_2(l_a, t) = w_3(l_a, t), \qquad \phi_2(l_a, t) = \phi_3(l_a, t), \qquad EI\phi_2'(l_a, t) = EI\phi_3'(l_a, t),$$
$$kaG(w_2'(l_a, t) - \phi_2(l_a, t)) = kaG(w_3'(l_a, t) - \phi_3(l_a, t)), \tag{12}$$

where the prime refers to the derivative of the function to x.

Substituting equations (7) and (8) into equations (11) and (12), the following matrix equations are obtained,

$$[\mathbf{T}_1]\begin{bmatrix} A_1 \\ B_1 \\ C_1 \\ D_1 \end{bmatrix} = [\mathbf{T}_{2L}]\begin{bmatrix} A_2 \\ B_2 \\ C_2 \\ D_2 \end{bmatrix} \quad \text{and} \quad [\mathbf{T}_{2R}]\begin{bmatrix} A_2 \\ B_2 \\ C_2 \\ D_2 \end{bmatrix} = [\mathbf{T}_3]\begin{bmatrix} A_3 \\ B_3 \\ C_3 \\ D_3 \end{bmatrix}, \tag{13, 14}$$

where

$$[\mathbf{T}_1] = \begin{bmatrix} 0 & 1 & 0 & 1 \\ q_{a1} & 0 & q_{b1} & 0 \\ 0 & -q_{a1}k_{a1} & 0 & q_{b1}k_{b1} \\ k_{a1} - q_{a1} & 0 & k_{b1} - q_{b1} & 0 \end{bmatrix}, \tag{15}$$

$$[\mathbf{T}_{2L}] = \begin{bmatrix} 0 & 1 & 0 & 1 \\ q_{a2} & 0 & q_{b2} & 0 \\ 0 & -q_{a2}k_{a2} & 0 & q_{b2}k_{b2} \\ k_{a2} - q_{a2} & 0 & k_{b2} - q_{b2} & 0 \end{bmatrix}, \tag{16}$$

$$[\mathbf{T}_{2R}] = \begin{bmatrix} \sin k_{a2}l_a & \cos k_{a2}l_a & \sinh k_{a2}l_a & \cosh k_{a2}l_a \\ q_{a2}\cos k_{a2}l_a & -q_{a2}\sin k_{a2}l_a & q_{b2}\cosh k_{b2}l_a & q_{b2}\sinh k_{b2}l_a \\ -q_{a2}k_{a2}\sin k_{a2}l_a & -q_{a2}k_{a2}\cos k_{a2}l_a & q_{b2}k_{b2}\sinh k_{b2}l_a & q_{b2}k_{b2}\cosh k_{b2}l_a \\ (k_{a2} - q_{a2})\cos k_{a2}l_a & -(k_{a2} - q_{a2})\sin k_{a2}l_a & (k_{b2} - q_{b2})\cosh k_{b2}l_a & (k_{b2} - q_{b2})\sinh k_{b2}l_a \end{bmatrix} \tag{17}$$

and

$$[\mathbf{T}_3] = \begin{bmatrix} \sin k_{a3}l_a & \cos k_{a3}l_a & \sinh k_{a3}l_a & \cosh k_{a3}l_a \\ q_{a3}\cos k_{a3}l_a & -q_{a3}\sin k_{a3}l_a & q_{b3}\cosh k_{b3}l_a & q_{b3}\sinh k_{b3}l_a \\ -q_{a3}k_{a3}\sin k_{a3}l_a & -q_{a3}k_{a3}\cos k_{a3}l_a & q_{b3}k_{b3}\sinh k_{b3}l_a & q_{b3}k_{b3}\cosh k_{b3}l_a \\ (k_{a3} - q_{a3})\cos k_{a3}l_a & -(k_{a3} - q_{a3})\sin k_{a3}l_a & (k_{b3} - q_{b3})\cosh k_{b3}l_a & (k_{b3} - q_{b3})\sinh k_{b3}l_a \end{bmatrix} \tag{18}$$

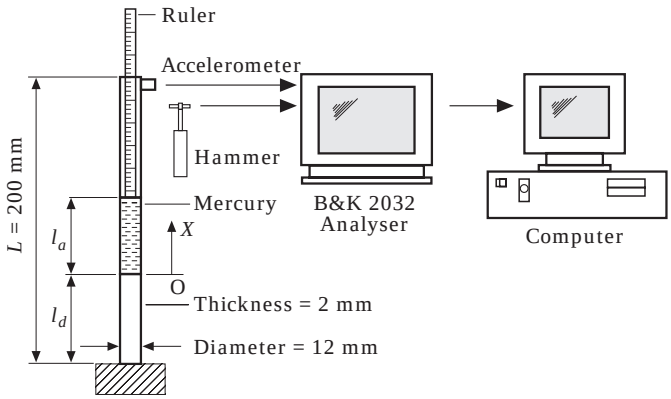

Figure 2. The experimental setup of a cantilever tube partially filled with mercury.

The boundary conditions yield,

$$[\mathbf{K}_1]\begin{bmatrix} A_1 \\ B_1 \\ C_1 \\ D_1 \end{bmatrix} + [\mathbf{K}_3]\begin{bmatrix} A_3 \\ B_3 \\ C_3 \\ D_3 \end{bmatrix} = 0 \tag{19}$$

where $[\mathbf{K}_1]$ and $[\mathbf{K}_3]$ are dependent on boundary conditions and their matrix forms can be found in the Appendix. As an example that is convenient for experimental data to be obtained, a cantilever Timoshenko beam is considered, as shown in Figure 2. Then,

$$[\mathbf{K}_1] = \begin{bmatrix} -\sin k_{a1}l_d & \cos k_{a1}l_d & -\sinh k_{b1}l_d & \cosh k_{b1}l_d \\ q_{a1}\cos k_{a1}l_d & q_{a1}\sin k_{a1}l_d & q_{b1}\cosh k_{b1}l_d & -q_{b1}\sinh k_{b1}l_d \\ 0 & 0 & 0 & 0 \\ 0 & 0 & 0 & 0 \end{bmatrix} \tag{20}$$

$$[\mathbf{K}_3] = \begin{bmatrix} 0 & 0 & 0 & 0 \\ 0 & 0 & 0 & 0 \\ -q_{a3}k_{a3}\sin k_{a3}(L-l_d) & -q_{a3}k_{a3}\cos k_{a3}(L-l_d) & q_{b3}k_{b3}\sinh k_{b3}(L-l_d) & q_{b3}k_{b3}\cosh k_{b3}(L-l_d) \\ (k_{a3}-q_{a3})\cos k_{a3}(L-l_d) & -(k_{a3}-q_{a3})\sin k_{a3}(L-l_d) & (k_{b3}-q_{b3})\cosh k_{b3}(L-l_d) & (k_{b3}-q_{b3})\sinh k_{b3}(L-l_d) \end{bmatrix} \tag{21}$$

By using equations (13) and (14), the coefficient vectors, $(A_1\ B_1\ C_1\ D_1)^T$ and $(A_2\ B_2\ C_2\ D_2)^T$ can be eliminated to give,

$$\{[\mathbf{K}_1][\mathbf{T}_1]^{-1}[\mathbf{T}_{2L}][\mathbf{T}_{2R}]^{-1}[\mathbf{T}_3] + [\mathbf{K}_3]\}\begin{bmatrix} A_3 \\ B_3 \\ C_3 \\ D_3 \end{bmatrix} = 0 \tag{22}$$

The roots of the determinant equation,

$$|[\mathbf{K}_1][\mathbf{T}_1]^{-1}[\mathbf{T}_{2L}][\mathbf{T}_{2R}]^{-1}[\mathbf{T}_3] + [\mathbf{K}_3]| = 0 \tag{23}$$

give the exact natural frequencies. The corresponding eigenvectors of equation (22) together with equations (13) and (14) determine the eigenfunctions in the form of equations (7) and (8). The eigenfunctions give the mode shapes of the loaded cantilever.

3. EXPERIMENT

3.1. EXPERIMENTAL SET-UP AND METHOD

Built-in and free-end supports are easier to set up experimentally. A cantilever tube was then built for the experiments. In Figure 2 is shown the aluminium cantilever tube which is 200 mm long, 2 mm thick and 12 mm in external diameter. Its density was measured to be 2892 kg/m^3. The Young's and the shear moduli of the tube material were measured by a frequency method. A slender rod of the same material was made. It was suspended horizontally by two flexible strings to form a free–free beam. The "pendulum" modes of the setup are so low that they do not affect the flexural modes. The first ten natural frequencies of the free–free beam were then measured by using a hammering method to be introduced later. The Young's modulus was determined as $6{\cdot}1802 \times 10^{10}$ N/m^2 from the fundamental frequency using the formula presented by Tefft [18]. (Because of the slenderness of the rod, the fundamental mode is assumed to be less influenced by the Timoshenko effect.) The shear modulus was determined to be $2{\cdot}5412 \times 10^{10}$ N/m^2 from all the ten natural frequencies by using the Timoshenko model. The least squares method was employed to obtain the best estimation of the constant.

A thin disc was made available to block a column of mercury within the tube to form a partial span of mass. Using the notations shown in the figure, $l_d = 60$ mm, and the mercury length l_a can be varied and measured by using a floating ruler. Careful check has been carried out, showing that the effect of the thin disc on natural frequencies and mode shapes of the tube is negligible. The damping ratio of the tube for the first mode was measured as $4{\cdot}08 \times 10^{-4}$ (empty) and $9{\cdot}87 \times 10^{-4}$ (with mercury, $0{\cdot}7L$), showing an increasing trend. However, the values do not appear to have appreciable effect on the measured free vibration frequency.

Natural frequencies and mode shapes of the partially filled tube were measured by the modal testing system shown in figure 2. The random series of impacts method introduced by Wong and Chan [19] was used in the measurement. The tube was excited by an instrumented hammer (B&K 8202), and a light-weight accelerometer (B&K 4374) was used to measure the response. The mass of the accelerometer was 0·65 g. Compared with the mass of the empty tube, 36·34 g, this would cause less than 1% frequency reduction when the accelerometer is placed at an anti-nodal position. Both excitation and response signals were amplified and transferred to a signal analyser (B&K 2032 with 801 lines) to calculate the frequency response function (FRF). The analyser was set to 50 samples on averaged mode, with Hanning smoothing and 75% overlapping. Using a modal analysis software (PC MODEL, VEC Inc.), natural frequencies and mode shapes of the first three modes were measured. Frequency were determined from the FRFs by the curve-fitting method, and mode shape data were calculated from a set of modal constants, which were also extracted from the FRFs. The method of "roving exciter" was employed in the experiment, where the output acceleration of the tube was recorded at a single stationary reference point (free end), and the tube was excited at a number of locations along the tube. For each value of mercury length, a set of FRFs were obtained for modal analysis.

3.2. EXPERIMENTAL RESULTS FOR VERIFICATION

Figures 3 and 4 show experimental results of natural frequency and mode shape of the cantilever tube, respectively, for different lengths of mercury. The corresponding computational results are also given in the figures for comparison. They are calculated based on the Euler–Bernoulli beam theory (Chan and Zhang, [7]) and the Timoshenko beam theory (present formulation), as differentiated by the solid and dotted lines respectively. It is seen from Figure 3 that the computational results based on Timoshenko theory agree quite well with experimental data. The results also show that the Euler–Bernoulli theory has over-estimated the natural frequencies of the cantilever tube. In other words, Timoshenko theory is a more accurate model, particularly evident for the third mode. It is noticeable that there is a disparity between the theoretical and measured natural frequencies of the beam without mercury. This can be attributed to the fact that it is difficult to make a perfect built-in support. For the mode shape measurements, Figure 4 shows that the third mode shapes for three different mercury lengths (length ratio equals 0·0, 0·2 and 0·7) agree well with the computed results by both theories. It can be seen that Euler–Bernoulli and Timoshenko beam theories predict almost similar mode shapes irrespective of the difference in the predicted natural frequencies.

A comparison between the present method and the finite element method (FEM) for calculating natural frequencies of the partially filled tube, as studied in the experiment, has also been made (results not presented here). The results by FEM are found to be consistent with those by the present method. The difference between them is reduced with increasing number of elements. Such difference is also found to increase with the mode number, but the maximum is within 1%, for the first three modes. It is found that FEM predicts higher values of natural frequencies. This is consistent with the fact that the present method predicts the exact (stationary) eigenvalues of the system.

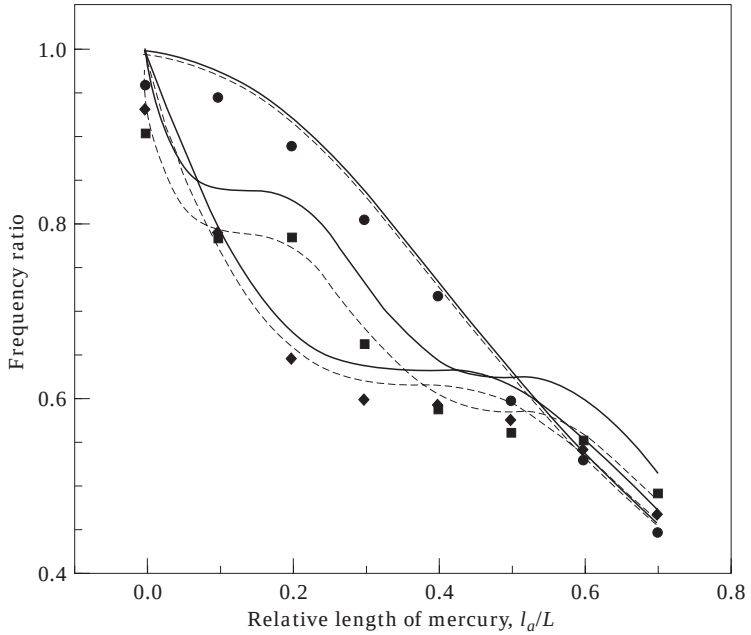

Figure 3. The frequency shift of the cantilever tube partially filled with mercury at $l_d/L = 0{\cdot}3$. ●●●, mode 1; ◆◆◆, mode 2; ■■■, mode 3. Key: solid curves are for Euler–Bernoulli theory; dashed curves for Timoshenko theory; symbols are experimental data.

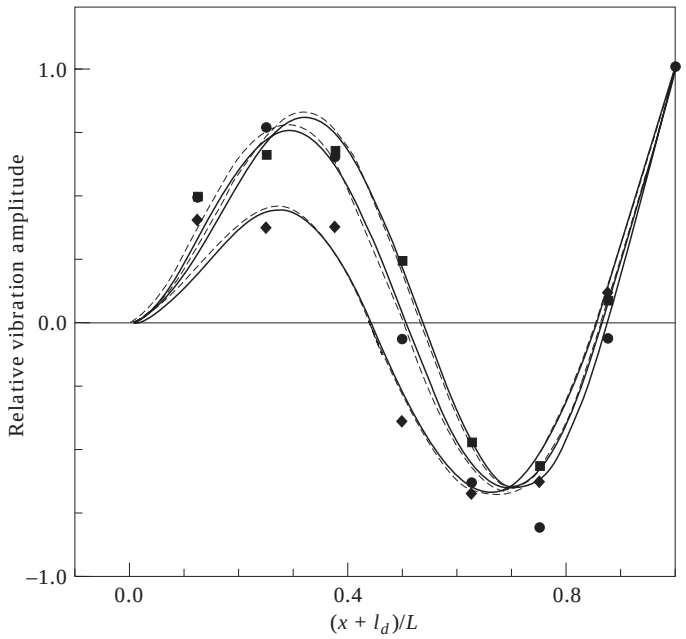

Figure 4. The third cantilever tube mode shapes with mercury at $l_d/L = 0{\cdot}3$. l_a/L values: ● ● ●, 0·0; ◆ ◆ ◆, 0.2; ■ ■ ■, 0·7. Key as for Figure 3.

4. COMPUTATIONAL RESULTS AND DISCUSSION

Since there are available data in the literature for a simply supported beam with concentrated mass for comparison, such a beam structure is used as an example here. As shown in Figure 1, the mass is assumed to be added symmetrically about the beam axis. When l_a becomes very small compared with L, the distributed mass can be considered as a concentrated one.

4.1. CONCENTRATED MASS LOAD

When $l_a/L = 0{\cdot}001$, the natural frequency as function of l_d calculated by equation (23) has been found to be almost similar to that when $l_a/L = 0{\cdot}01$. For comparison with Grant [6], when the load is at the mid point of the beam, the natural frequencies as a function of radius of gyration r_g, where $r_g = \sqrt{I/a}$, is given in Figure 5. The parameters used in the computation are the same as those in Grant [6]. The present results agree very well with the data extracted from Grant [6], indicating that the present general model predicts results of Grant's particular case.

4.2. DISTRIBUTED MASS LOAD

In Figure 6 is shown the frequency curves as the functions of position of the mass centre. Frequency values are scaled by the corresponding modal values of the unloaded Timoshenko beam. Let D be the diameter of the circular beam used in this example and L its length. Assume that $D/L = 0{\cdot}1$, and Poisson's ratio, $\gamma = 0{\cdot}345$. According to Cowper [11], the shear coefficient for a circular section, $k = 6(1 + \gamma)/(7 + 6\gamma) = 0{\cdot}89$. Initially, let the length be fixed at $l_a/L = 0{\cdot}1$, and $m_a/m = 10$. Figure 6 gives the modal frequency curves for mode numbers 1, 2, 3 and 6, showing peak and trough features.

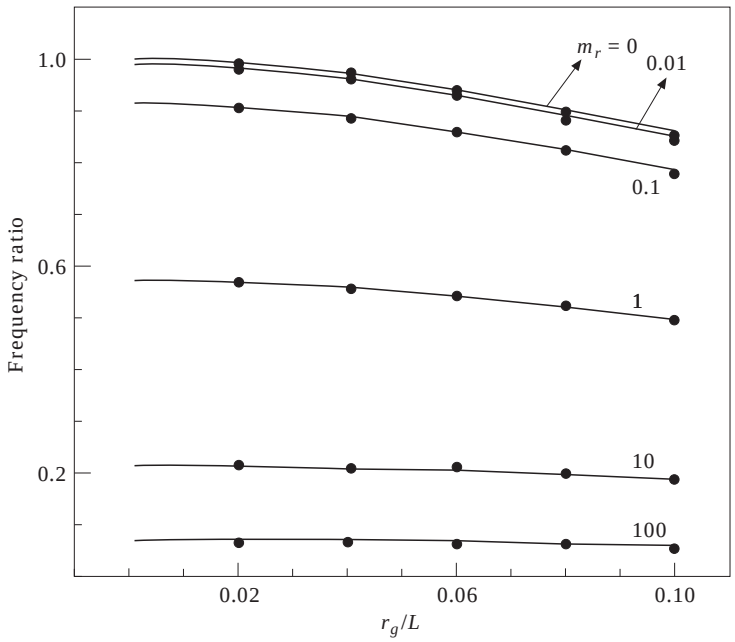

Figure 5. The frequency shift of the beam in Figure 1 with simply-supported ends. $l_a/L = 0{\cdot}001$ and $l_a/L = 0{\cdot}4995$. m_r is the ratio of added mass to beam mass. Symbols are data reproduced from Grant [6] with courtesy.

In the figure is shown three points on the curve of the third mode. They are marked as A, B and C, respectively representing the peak, minimum and median frequency values for some specific positions of the mass. At these positions, the third normal mode shapes and bending slope curves are shown in Figures 7a and 7b, respectively.† One observes that the bending slope varies slightly compared with significant variation of the mode shape. From Figure 7a, it can be seen that the nodal points shift with mass position, in a "swinging" manner. As the mass centre is located at positions B or C, it coincides with a position other than the node of the affected mode. The amplitude of the mode shape is locally reduced, but its maximum increased, compared with that when the mass centre is at position A. When the mass centre is situated at a node, the normalized mode shape is more regular.

4.3. INFLUENCES OF DISTRIBUTED MASS LENGTH AND DENSITY

Three possible cases are studied;

Case 1: l_a/L varies while m_a/m remains constant;

Case 2: l_a/L varies while the distributed mass, $m_a l_a$, remains constant;

Case 3: m_a/m varies while l_a/L remains constant.

For these three cases, the frequency shift curves for the third vibrating mode as function of the position of mass centre are shown in Figure 8 ($l_a/L = 0{\cdot}05$, $0{\cdot}10$, $0{\cdot}16$ and $0{\cdot}20$ while $m_a/m = 10$), Figure 9 ($l_a/L = 0{\cdot}05$, $0{\cdot}10$, $0{\cdot}15$ and $0{\cdot}40$ while $m_a l_a/mL = 2$), and Figure 10

†The normal vibrating modes are obtained by the following normalization process, i.e. let

$$\int_{-l_d}^{L-l_d} \left\{ EI \frac{d\Phi_i(x)}{dx} \frac{d\Phi_i(x)}{dx} + kaG \left(\frac{dW_i(x)}{dx} - \Phi_i(x) \right) \left(\frac{dW_j(x)}{dx} - \Phi_j(x) \right) \right\} dx = \delta_{ij},$$

$i, j = 1, 2, 3, \ldots$

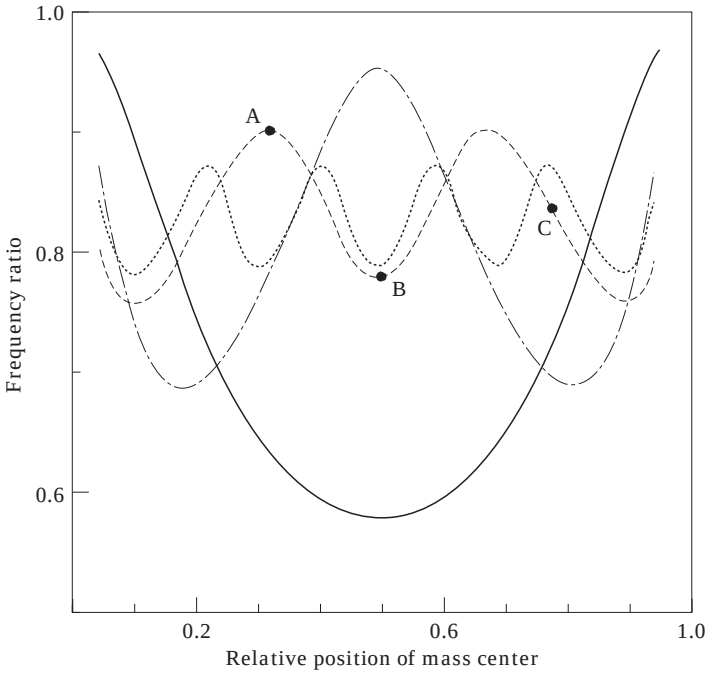

Figure 6. The frequency shift of the beam in Figure 1 with simply-supported ends. $l_a/L = 0{\cdot}1$, $m_a/m = 10$ and $D/L = 0{\cdot}1$. ——, mode 1; – · – · –, mode 2; – – – – – –. mode 3; --------, mode 6.

($m_a/m = 10$, 20, 33 and 50 while $l_a/L = 0{\cdot}1$) respectively. In Figure 8 are show two groups of points, marked as solid and hollow circles for later use.

A common and noticeable feature is that there exist certain values of l_a/L (Cases 1 and 2) or m_a/m (Case 3), where the frequency is not sensitive to the mass centre position. From the figure, it can be seen that at those values of l_a/L or m_a/m, the frequency shift curves change in shape, appearing as "transitions" from one shape to other. The frequency curves appear to be mirror images about the "plateau" line. This feature can be interpreted in terms of energy distributions.

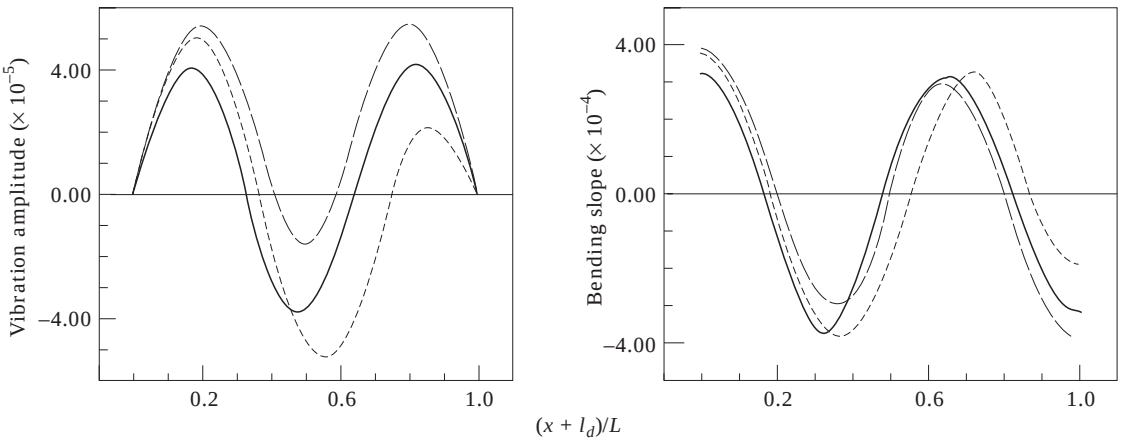

Figure 7. The third normal mode shapes of the beam in Figure 1 with simply-supported ends. $m_a/m = 10$, $D/L = 0{\cdot}1$ and $l_a/L = 0{\cdot}1$. ——, at position A; – – – – – –, B; --------, C as indicated in Figure 6. (a) for transverse, W; (b) for bending slope, Φ.

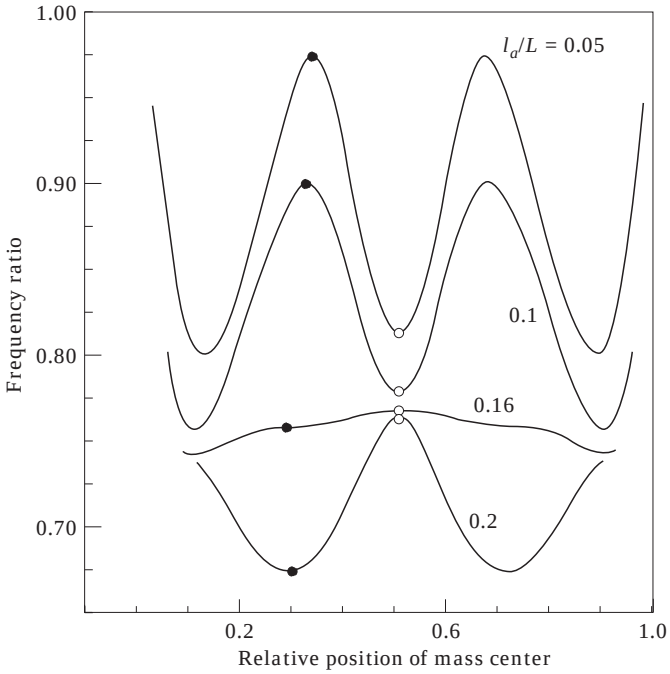

Figure 8. The frequency shift of the beam in Figure 1 with simply-supported ends. $m_a/m = 10$ and $D/L = 0{\cdot}1$ for different values of mass length, l_a/L. Solid circles are Group A data and hollow circles Group B.

Using Case 1 (Figure 8) as an example, consider the energy distributions between beam strain, beam kinetic and mass kinetic energies. All mode shapes are normalized to make maximum potential energy unity. Thus, the square of the circular natural frequency will be inversely proportional to the maximum reference kinetic energy, written as

$$T^* = T^*_{beam} + T^*_{mass} = \int_{-l_d}^{L-l_d} \left\{ mW^2(x) + \frac{mI}{a}\Phi^2(x) \right\} \mathrm{d}x + \int_0^{l_a} \left\{ m_a W^2(x) + \frac{m_a I}{a}\Phi^2(x) \right\} \mathrm{d}x \tag{23}$$

where T^*_{beam} and T^*_{mass} are the parts of the beam and the mass, respectively.

In Figure 11 is shown the distributions of T^*_{beam} and T^*_{mass} as function of mass centre position, for $l_a/L = 0{\cdot}05$, $0{\cdot}1$, $0{\cdot}16$ and $0{\cdot}2$. Two groups of curves appear, top ones for T^*_{beam} and bottom ones for T^*_{mass}, as indicated in the figure.

For various values of l_a/L, T^*_{beam} curves show little change compared with T^*_{mass} ones. For $l_a/L = 0{\cdot}1$, T^*_{beam} is minimum when the mass centre is located at a node, and maximum at an anti-node. The former effect is expected to be less effective in reducing frequency and the latter more effective. It can be seen in Figures 7a and 7b that the change of the beam kinetic energy is due to the change of mode shapes rather than their slopes.

T^*_{mass} curves shown in Figure 11 appear to be more sensitive to change in mass length ratio. Computational results show translate inertia is more dominant than the rotary inertia in affecting T^*_{mass}.

In Figure 12 is shown the normal mode shapes for $l_a/L = 0{\cdot}05$, $0{\cdot}1$, $0{\cdot}16$ and $0{\cdot}2$ for mass positions A and B (refer to figure 8). When l_a/L is equal to $0{\cdot}05$, T^*_{mass} is maximum at position B and minimum at position A. The T^*_{mass} curve appears to be of the same "phase" as that of the T^*_{beam} curve. When the ratio is increased to $0{\cdot}1$, at position B, the added mass

laps the nodes at two sides of the mode and the vibration amplitude is reduced locally. At position A, the distributed mass of 0.1 covers the antinodes at two sides. At these two positions T^*_{mass} is almost equal. It can be seen in Figure 11 that the T^*_{mass} curve is like a plateau. Increasing l_a/L further, T^*_{mass} curves shift up with a larger range of fluctuations. The curve shape appears to be out of "phase" with that of the T^*_{beam} curve.

Therefore, it is not difficult to explain the plateau curve of Figure 8. When l_a/L equals 0·16, the T^*_{mass} curve is out of phase with that of T^*_{beam}. The sum of them is T^* curve in a shape of an inverted plateau, resulting in the frequency plateau curve of Figure 8. Thus, before the transition, the frequency curve shape is governed by the beam inertia. After that, it is dominated by the added mass inertia.

For Cases 2 and 3, the above argument is also valid. Thus for a beam–mass system, it is possible to obtain an arrangement that is not sensitive to a change in mass position. This can be of value in solving practical engineering problems, perhaps particularly useful for analyzing vibration of beams with a traversing mass.

4.4. THE VALIDITY OF EULER–BERNOULLI THEORY FOR THE MASS-LOADED BEAM

It may also be useful to give some indication of the validity of Euler–Bernoulli theory for the mass-loaded beam. Some computational work has been conducted on the error of the Euler–Bernoulli theory for the mass-loaded simply-supported beam, compared with Timoshenko theory. It is shown that besides the effect of the mode number and the radius of gyration–length ratio of the beam (r_g/L), the error also depends on the parameters of the added mass, such as the mass ($m_r = m_a/m$), the mass length (l_a/L) and the mass position (l_d/L). From our results (not presented here), for the fundamental mode, the effect of such parameters is relatively slight (the error is below 2%). For the higher modes, the error appears to be higher (up to 7% for the second mode and 18% for the third). Thus, there is no general rule with regard to when Euler–Bernoulli theory could be used instead of

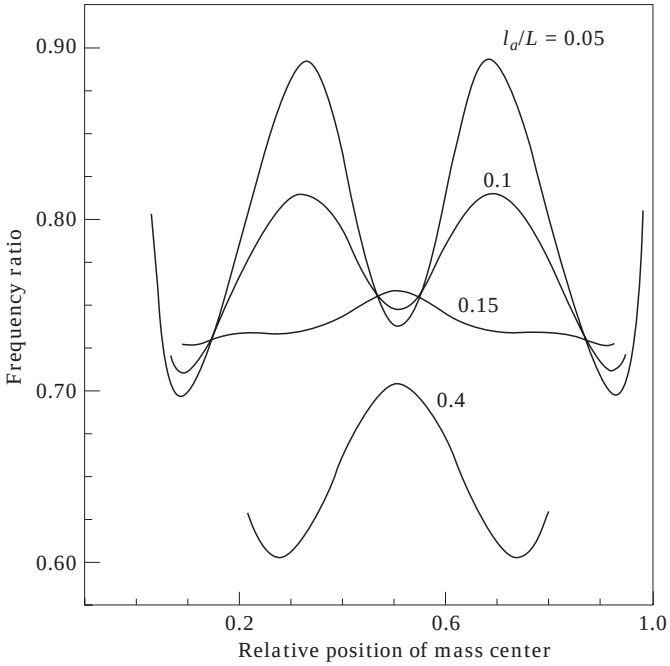

Figure 9. The frequency shift of the beam in Figure 1 with simply-supported ends. $m_a\, l_a/mL = 2$ and $D/L = 0{\cdot}1$ for different values of mass length, l_a/L.

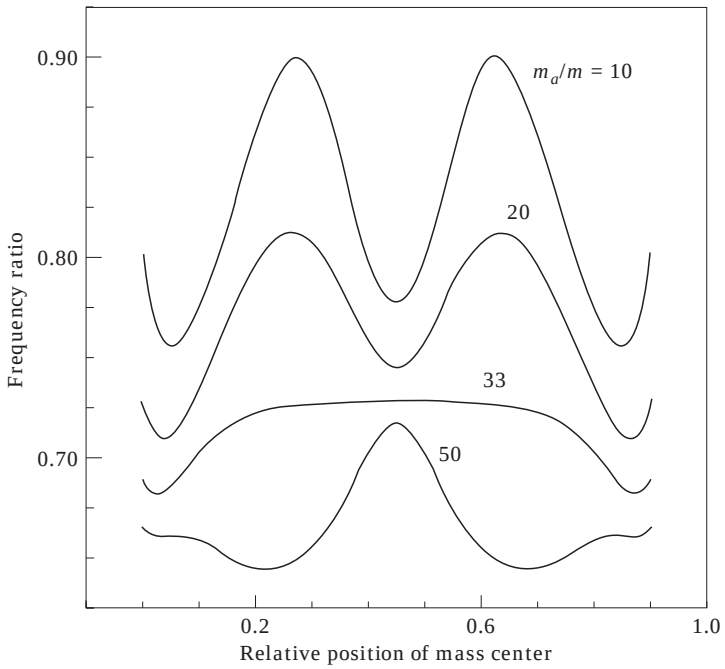

Figure 10. The frequency shift of the beam in Figure 1 with simply-supported ends. $D/L = 0{\cdot}1$ and $l_a/L = 0{\cdot}1$ for different values of density ratio, m_a/m.

Timoshenko theory for the studied beam. Compared with Timoshenko theory, the error of Euler–Bernoulli theory is actually due to disregarding the effect of rotary inertia and shear deformation. For uniform beams, the effect of shear deformation is the major factor for the reduction in natural frequency, as pointed out by Timoshenko himself [3]. However, for the mass-loaded beam, the effect of rotary inertia and shear deformation is found to vary with the aforementioned mass parameters, and when the added mass is located at some position or its length is of a certain value, the effect of rotary inertia becomes more predominant than that of shear deformation.

5. CONCLUSIONS

An exact solution to a free vibration problem of a Timoshenko beam partially loaded with a distributed mass over an intermediate span has been obtained for different boundary conditions. The natural frequencies and normal mode shapes were calculated. An experiment has also been carried out to verify the data. It was found that the present Timoshenko beam model yields more accurate natural frequencies than the Euler–Bernoulli theory, especially for higher modes. The model could also be used for a beam with a concentrated load, with the results calculated appearing to be consistent with those of another investigator.

Some interesting computational results were obtained. It was found that there was no frequency change for certain values of added mass position, length and/or density. For other values, however, the change appeared to be cyclical with amplitude depending on the inertia of the added mass. Through the analysis of energy distributions, such feature was found to be mainly due to translatory motion of the mode but not to the rotary one. This can be of value in solving practical engineering problems, perhaps particularly useful

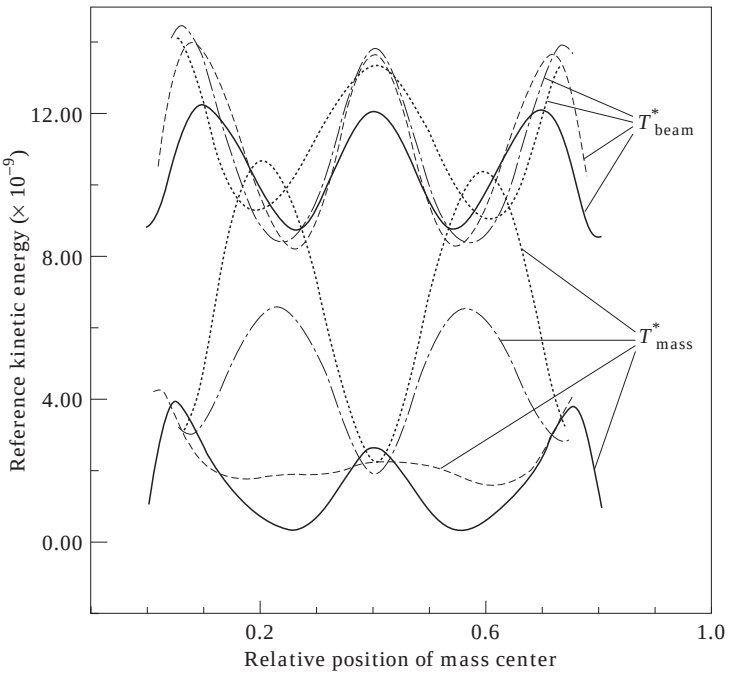

Figure 11. Curves of reference kinetic energy of the beam in Figure 1 with simply-supported ends. $m_a/m = 10$ and $D/L = 0{\cdot}1$. l_a/L values: ——, 0·05; – – – –. 0·1; – · – · –, 0·16; --------, 0·2.

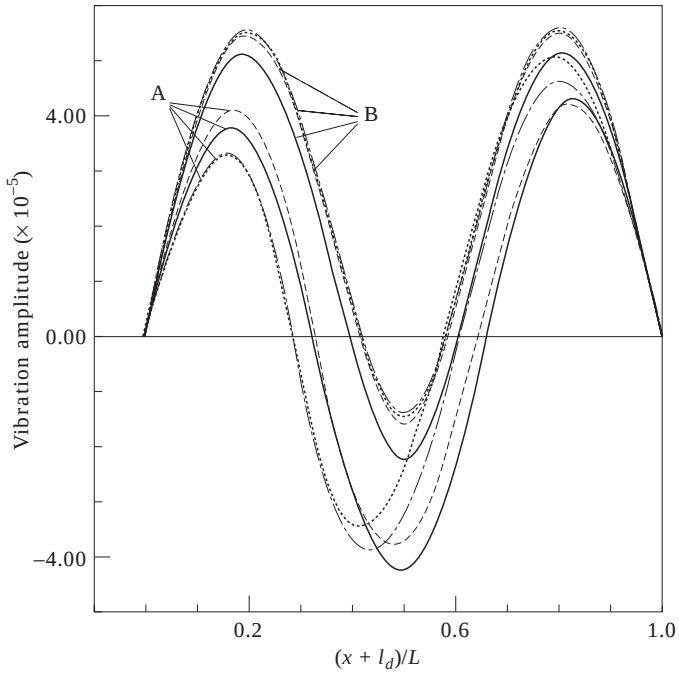

Figure 12. The third mode shapes of the beam in Figure 1 with simply-supported ends at groups A B positions as shown in Figure 8. $m_a/m = 10$, $D/L = 0{\cdot}1$. l_a/L values: ——, 0·05; – – – –, 0·1; – · – · –, 0·16; --------, 0·2.

for analyzing the vibration of beams with traversing mass. For the mass-loaded beam, the effect of rotary inertia and shear deformation was found to vary with the mass parameters, and sometimes the effect of rotary inertia became predominant.

ACKNOWLEDGMENT

Gratitude is due to The Hong Kong Polytechnic University for the continuing financial support of this research, to Professor S. R. Reid of UMIST for his comments on certain aspects of this research work, and to the China Light and Power Company Limited for their assistance in carrying out the experiments.

REFERENCES

1. Lord Rayleigh 1945 *Theory of Sound* (two volumes). New York: Dover Publications, second edition.
2. S. P. Timoshenko 1921 *Philosophical Magazine*, series 6, **41**, 744–746. On the correction for shear of the differential equation for transverse vibrations of prismatic bars.
3. S. P. Timoshenko 1922 *Philosophical Magazine*, series 6, **43**, 125–131. On the transverse vibrations of bars of uniform cross sections.
4. P. W. Traill-Nash and A. R. Collar 1953 *Quarterly Journal of Mechanics and Applied Mathematics* **6**, 186–222. The effects of shear flexibility and rotatary inertia on the bending vibrations of beams.
5. T. C. Huang 1961 *American Society of Mechanical Engineers*, *Journal of Applied Mechanics* **28**, 579–584. The effect of rotary inertia and of shear deformation on the frequency and normal mode equations of uniform beams with simple end conditions.
6. D. A. Grant 1978 *Journal of Sound and Vibration* **57**, 357–365. The effect of rotary inertia and shear deformation on the frequency and normal mode equations of uniform beams carrying a concentrated mass.
7. K. T. Chan and J. Z. Zhang 1995 *Journal of Sound and Vibration* **182**, 185–190. Free vibration of a cantilever tube partially filled with liquid.
8. K. T. Chan, T. P. Leung and W. O. Wong 1996 *Journal of Sound and Vibration* **191**, 590–597. Free vibration of simply supported beam partially loaded with distributed mass.
9. G. Pickett 1945 *Journal of Applied Physics* **16**, 820–831. Flexural vibration of unrestrained cylinders and disks.
10. R. D. Mindlin and H. Deresiewicz 1954 *Proceedings of the second U.S. National Congress of Applied Mechanics* 175–178. Timoshenko's shear coefficient for flexural vibrations of beams.
11. G. R. Cowper 1966 *American Society of Mechanical Engineers*, *Journal of Applied Mechanics* **33**, 335–340. The shear coefficient in Timoshenko's beam theory.
12. B. Aalami and B. Atzori 1974 *American Institute of Aeronautics and Astronautics Journal* **12**, 679–685. Flexural vibrations and Timoshenko's beam theory.
13. Y. W. Hsu 1975 *American Society of Mechanical Engineers*, *Journal of Applied Mechanics* **42**, 226–228. The shear coefficient of beams of circular cross section.
14. T. Kaneko 1975 *Journal of Physics D*: *Applied Physics* **8**, 1927–1936. On Timoshenko's correction for shear in vibrating beams.
15. N. G. Stephen 1978 *American Society of Mechanical Engineers*, *Journal of Applied Mechanics* **45**, 695–697. On the variation of Timoshenko's shear coefficient with frequency.
16. N. G. Stephen 1980 *American Society of Mechanical Engineers*, *Journal of Applied Mechanics* **47**, 121–127. Timoshenko's shear coefficient from a beam subjected to gravity loading.
17. J. J. Jensen 1983 *Journal of Sound and Vibration* **87**, 621–635. On the shear coefficient in Timoshenko's beam theory.
18. W. E. Tefft 1960 *Journal of Research of the National Bureau of Standards-B. Mathematics and Mathematical Physics* 64B, 237–242. Numerical solution of the frequency equations for the flexural vibration of cylindrical rods.
19. C. N. Wong and K. T. Chan 1996 *American Society of Mechanical Engineers*, *Journal of Vibration and Acoustics* (accepted). Identification of vibration of cooler tubes with tube-to-baffle impactions.

APPENDIX: MATRIX EXPRESSION FOR SEVERAL COMMON CLASSICAL BOUNDARY CONDITIONS

A.1. FREE–FREE

$$EI\,\mathrm{d}\Phi_1(-l_d)/\mathrm{d}x = 0, \qquad kaG[\mathrm{d}W_1(-l_d)/\mathrm{d}x - \Phi_1(-l_d)] = 0,$$
$$EI\,\mathrm{d}\Phi_3(L-l_d)/\mathrm{d}x = 0, \qquad kaG[\mathrm{d}W_3(L-l_d)/\mathrm{d}x - \Phi_3(L-l_d)] = 0,$$

$$[\mathbf{K}_1] = \begin{bmatrix} q_{a1}k_{a1}\sinh k_{a1}(l_d) & -q_{a1}k_{a1}\cos k_{a1}(l_d) & -q_{b1}k_{b1}\sinh k_{b1}(l_d) & q_{b1}k_{b1}\cosh k_{b1}(l_d) \\ (k_{a1}-q_{a1})\cos k_{a1}(kl_d) & (k_{a1}-q_{a1})\sin k_{a1}(l_d) & (k_{b1}-q_{b1})\cosh k_{b1}(l_d) & -(k_{b1}-q_{b1})\sinh k_{b1}(l_d) \\ 0 & 0 & 0 & 0 \\ 0 & 0 & 0 & 0 \end{bmatrix},$$

$$[\mathbf{K}_3] = \begin{bmatrix} 0 & 0 & 0 & 0 \\ 0 & 0 & 0 & 0 \\ -q_{a3}k_{a3}\sin k_{a3}(L-l_d) & -q_{a3}k_{a3}\cos k_{a3}(L-l_d) & q_{b3}k_{b3}\sinh k_{b3}(L-l_d) & q_{b3}k_{b3}\cosh k_{b3}(L-l_d) \\ (k_{a3}-q_{a3})\cos k_{a3}(L-l_d) & -(k_{a3}-q_{a3})\sin k_{a3}(L-l_d) & (k_{b3}-q_{b3})\cosh k_{b3}(L-l_d) & (k_{b3}-q_{b3})\sinh k_{b3}(L-l_d) \end{bmatrix}.$$

A.2. CLAMPED–FREE (CANTILEVER)

$$W_1(-l_d) = 0, \qquad \Phi_1(-l_d) = 0, \qquad EI\,\mathrm{d}\Phi_3(L-l_d)/\mathrm{d}x = 0,$$
$$kaG[\mathrm{d}W_3(L-l_d)/\mathrm{d}x - \Phi_3(L-l_d)] = 0,$$

$$[\mathbf{K}_1] = \begin{bmatrix} -\sin k_{a1}l_d & \cos k_{a1}l_d & -\sinh k_{b1}l_d & \cosh k_{b1}l_d \\ q_{a1}\cos k_{a1}l_d & q_{a1}\sin k_{a1}l_d & q_{b1}\cosh k_{b1}l_d & -q_{b1}\sinh k_{b1}l_d \\ 0 & 0 & 0 & 0 \\ 0 & 0 & 0 & 0 \end{bmatrix}$$

$$[\mathbf{K}_3] = \begin{bmatrix} 0 & 0 & 0 & 0 \\ 0 & 0 & 0 & 0 \\ -q_{a3}k_{a3}\sin k_{a3}(L-l_d) & -q_{a3}k_{a3}\cos k_{a3}(L-l_d) & q_{b3}k_{b3}\sinh k_{b3}(L-l_d) & q_{b3}k_{b3}\cosh k_{b3}(L-l_d) \\ (k_{a3}-q_{a3})\cos k_{a3}(L-l_d) & -(k_{a3}-q_{a3})\sin k_{a3}(L-l_d) & (k_{b3}-q_{b3})\cosh k_{b3}(L-l_d) & (k_{b3}-q_{b3})\sinh k_{b3}(L-l_d) \end{bmatrix}.$$

A.3. SIMPLE–SIMPLE (SIMPLY-SUPPORTED)

$$W_1(-l_d) = 0, \qquad EI\,\mathrm{d}\Phi_1(-l_d)/\mathrm{d}x = 0, \qquad W_3(L-l_d) = 0, \qquad EI\,\mathrm{d}\Phi_3(L-l_d)/\mathrm{d}x = 0,$$

$$[\mathbf{K}_1] = \begin{bmatrix} -\sin k_{a1}l_d & \cos k_{a1}l_d & -\sinh k_{b1}l_d & \cosh k_{b1}l_d \\ q_{a1}k_{a1}\sin k_{a1}l_d & -q_{a1}k_{a1}\cos k_{a1}l_d & -q_{b1}k_{b1}\sinh k_{b1}l_d & q_{b1}k_{b1}\cosh k_{b1}l_d \\ 0 & 0 & 0 & 0 \\ 0 & 0 & 0 & 0 \end{bmatrix}$$

$$[\mathbf{K}_3] = \begin{bmatrix} 0 & 0 & 0 & 0 \\ 0 & 0 & 0 & 0 \\ \sin k_{a3}(L-l_d) & \cos k_{a3}(L-l_d) & \sinh k_{b3}(L-l_d) & \cosh k_{b3}(L-l_d) \\ -q_{a3}k_{a3}\sin k_{a3}(L-l_d) & -q_{a3}k_{a3}\cos k_{a3}(L-l_d) & q_{b3}k_{b3}\sinh k_{b3}(L-l_d) & q_{b3}k_{b3}\cosh k_{b3}(L-l_d) \end{bmatrix}.$$

A.4. CLAMPED–SIMPLE

$$W_1(-l_d) = 0, \qquad \Phi_1(-l_d) = 0, \qquad W_3(L - l_d) = 0, \qquad EI\,\mathrm{d}\Phi_3(L - l_d)/\mathrm{d}x = 0,$$

$$[\mathbf{K}_1] = \begin{bmatrix} -\sin k_{a1} l_d & \cos k_{a1} l_d & -\sinh k_{b1} l_d & \cosh k_{b1} l_d \\ q_{a1} \cos k_{a1} l_d & q_{a1} \sin k_{a1} l_d & q_{b1} \cosh k_{b1} l_d & -q_{b1} \sinh k_{b1} l_d \\ 0 & 0 & 0 & 0 \\ 0 & 0 & 0 & 0 \end{bmatrix},$$

$$[\mathbf{K}_3] = \begin{bmatrix} 0 & 0 & 0 & 0 \\ 0 & 0 & 0 & 0 \\ \sin k_{a3}(L - l_d) & \cos k_{a3}(L - l_d) & \sinh k_{b3}(L - l_d) & \cosh k_{b3}(L - l_d) \\ -q_{a3} k_{a3} \sin k_{a3}(L - l_d) & -q_{a3} k_{a3} \cos k_{a3}(L - l_d) & q_{b3} k_{b3} \sinh k_{b3}(L - l_d) & q_{b3} k_{b3} \cosh k_{b3}(L - l_d) \end{bmatrix}.$$

A.5. CLAMPED–CLAMPED

$$W_1(-l_d) = 0, \qquad \Phi_1(-l_d) = 0, \qquad W_3(L - l_d) = 0, \qquad \Phi_3(L - l_d) = 0,$$

$$[\mathbf{K}_1] = \begin{bmatrix} -\sin k_{a1} l_d & \cos k_{a1} l_d & -\sinh k_{b1} l_d & \cosh k_{b1} l_d \\ q_{a1} \cos k_{a1} l_d & q_{a1} \sin k_{a1} l_d & q_{b1} \cosh k_{b1} l_d & -q_{b1} \sinh k_{b1} l_d \\ 0 & 0 & 0 & 0 \\ 0 & 0 & 0 & 0 \end{bmatrix},$$

$$[\mathbf{K}_3] = \begin{bmatrix} \sin k_{a3}(L - l_d) & \cos k_{a3}(L - l_d) & \sinh k_{b3}(L - l_d) & \cosh k_{b3}(L - l_d) \\ q_{a3} \cos k_{a3}(L - l_d) & -q_{a3} \sin k_{a3}(L - l_d) & q_{b3} \cosh k_{b3}(L - l_d) & q_{b3} \sinh k_{b3}(L - l_d) \\ 0 & 0 & 0 & 0 \\ 0 & 0 & 0 & 0 \end{bmatrix}.$$